Journal of Intelligent Material Systems and Structures
http://jim.sagepub.com/

Nonlinear Finite Element Simulation of Shape Adaptive Structures with SMA Strip Actuator

Jin-Ho Roh, Jae-Hung Han and In Lee

Journal of Intelligent Material Systems and Structures 2006 17: 1007
DOI: 10.1177/1045389X06063084

The online version of this article can be found at:
http://jim.sagepub.com/content/17/11/1007

Published by:
SAGE
http://www.sagepublications.com

Additional services and information for *Journal of Intelligent Material Systems and Structures* can be found at:

Email Alerts: http://jim.sagepub.com/cgi/alerts

Subscriptions: http://jim.sagepub.com/subscriptions

Reprints: http://www.sagepub.com/journalsReprints.nav

Permissions: http://www.sagepub.com/journalsPermissions.nav

Citations: http://jim.sagepub.com/content/17/11/1007.refs.html

Downloaded from jim.sagepub.com at KAIST GRADUATE SCHOOL OF MGMT on April 19, 2011

Nonlinear Finite Element Simulation of Shape Adaptive Structures with SMA Strip Actuator

JIN-HO ROH, JAE-HUNG HAN* AND IN LEE

Department of Aerospace Engineering, Korea Advanced Institute of Science and Technology
373-1 Guseong-dong, Yuseong-gu, Daejeon, 305-701, Korea

ABSTRACT: In this research, the thermomechanical responses of shape memory alloy (SMA) actuators and their applications in the shape adaptive structures combining strip SMA actuators are investigated. The numerical algorithm of the three-dimensional (3-D) SMA thermomechanical constitutive equations based on Lagoudas model is developed to analyze the unique characteristics of a SMA strip. The Green–Lagrange strain-displacement relationships are adopted to consider the large displacements, large strains, and material nonlinearity. For the numerical results presented in this article, the ABAQUS finite element program has been utilized with an appropriate user supplied subroutine (UMAT) written by FORTRAN for modeling a SMA strip and host elastic structure elements. In this model of a SMA strip, the shape memory effect is restricted to one-way applications. Numerical results show that an SMA strip actuator can generate enough recovery force to deform the host structure and sustain the deformed shape subjected to large external load, simultaneously. But, there are some difficulties found in designing reversible shape adaptive structures with this actuator, even if the SMA strip is coupled to an elastic structure which compels the SMA to recover the initial condition.

Key Words: thermomechanical response, SMA, adaptive structures.

INTRODUCTION

INCREASED demands for improving the structural performance with recent advances in material science have produced smart structures which include the ability to sense, diagnose, and actuate in order to effectively perform desired functions. Some materials of interest in the development of smart structures are piezoelectric crystals, electrostrictive, and magnetostrictive materials, shape memory alloys, electrorheological fluids, and optical fibers. Compared with piezoelectric, electrostrictive and magnetostrictive compounds, shape memory alloys (SMA) are relative newcomers to the arena of smart materials.

The SMAs are characterized by solid state transformation between austenite and martensite phases in response to mechanical and thermal loadings. This provides the SMAs with the capability for sustaining and recovering transformation strain up to 10% which imbues them with unique actuator and potential sensor capabilities in smart structural systems. The inherent thermal–mechanical coupling and hysteresis associated with the phase transformations also pose significant modeling challenges which must be implemented to investigate the capabilities of SMAs as actuators or sensors. Several mathematical models that reproduce the SMA constitutive behavior have been proposed in the last two decades. The majority of the constitutive models reported in the research of SMA modeling can be formally classified into one of the two groups: micromechanics-based models and phenomenological models. The essence of the micromechanics-based models is in the modeling of the single grain and further averaging of the results over a representative volume element (RVE) to obtain a polycrystalline response of the SMAs. The micromechanics-based models were developed using the thermodynamic framework and micromechanics of a single crystal, and evaluating the energies involved during the phase transformations. Moreover, these models adopt homogenization techniques to derive the overall behavior of the SMA (Sun and Hwang, 1993a, b). The advantage of the micromechanics models is their ability to predict the effective material response with only crystal lattice parameters and the information from the martensitic transformation at the crystalline and grain levels. However, these models are complex and require a large number of numerical computations. On the other hand, in the phenomenological models, a macroscopic free energy

*Author to whom correspondence should be addressed.
E-mail: jaehunghan@kaist.ac.kr
Figures 4, 5, 8, 15, 16, 21, 22, 25 and 26 appear in color online: http://jim.sagepub.com

1045-389X/06/11 1007–16 $10.00/0 DOI: 10.1177/1045389X06063084
© 2006 SAGE Publications

Downloaded from jim.sagepub.com at KAIST GRADUATE SCHOOL OF MGMT on April 19, 2011

function that depends on internal variables and their evolution equations are usually postulated and used in conjunction with the second law of the thermodynamics to derive constraints on the constitutive behavior of the SMAs. This model does not directly depend on the behavior of the material at the microscopic level. But this approach is useful for engineering applications because of the relative simplicity of implementation in computational procedures. In particular, Liang and Rogers (1990) have developed an empirically based cosine model to represent the martensite fraction as a function of stress and temperature during transformation. But this model has a limitation to investigate the behavior of SMAs below some range of temperature. Brinson (1993) modified the Liang model and could predict the thermomechanical response of SMAs with more general cases. Some three-dimensional (3-D) models from this group have been derived by the generalization of 1-D results. Boyd and Lagoudas (1996) proposed the unified thermodynamic constitutive model for SMA materials based on the thermodynamic framework. By using a free energy function and dissipation potential, pseudoelasticity and shape memory effect are modeled accounting for 3-D transformation. Qidwai and Lagoudas (2000) presented a consistent thermodynamical model based on the principle of maximum dissipation transformation considering generalized transformation function. A comprehensive study on the numerical implementation of SMA thermomechanical constitutive response using elastic predictor-transformation corrector algorithms was presented.

As SMAs can sustain large forces and displacements, alter their shape, and change their stiffness and damping characteristics with temperature or applied load, they have been excellent candidates for adaptive or smart structural systems. Roh and Kim (2003) considered a low velocity impact for the hybrid smart plate. The hybrid smart plate using SMA actuators and piezoelectric sensors can enhance its global resistance to low velocity impact. Lee et al. (2003) investigated the thermomechanical responses of SMA hybrid composite shell panel. The numerical results showed that SMA actuator could enhance the structural stiffness and suppress thermally buckled deflection of the composite shell panel. Marfia et al. (2003) investigated the behavior of SMA laminated beams. The numerical results demonstrated that the SMA actuators are very effective to change the shape of beam structure by performing temperature cycles on the SMA layers. The high work density to weight ratio of SMAs makes them ideal candidates for a variety of aerospace applications. In the 1995 Smart Wing Program, SMA torque tubes were employed to modify aerodynamic properties of an airfoil to increase lift and rolling moments. Singh et al. (2003) described the design, analysis, and testing of an improved SMA based tracking tab actuator for a helicopter rotor to minimize vibration due to rotor dissimilarities. Kudva (2004) illustrated the potential of bulk SMA to improve flight characteristics within the constraint mandated by low switching frequencies.

In this study, the thermomechanical responses of SMA actuators and their applications in the shape adaptive structures are investigated. The numerical algorithm of the 3-D SMA thermomechanical constitutive equations based on Lagoudas model is developed to analyze the unique characteristics of a SMA strip such as the pseudoelastic behavior and shape memory effect. The incremental SMA constitutive equations are implemented in the user supplied subroutine UMAT by using ABAQUS finite element program. In the finite element modeling, The Green–Lagrange strain-displacement relationships are adopted to consider the large displacements, large strains, and material nonlinearity. The interactions between host structure and a SMA strip actuator and the actuator characteristic such as how magnitude of recovery stress can be generated by heating and cooling cycle are investigated by considering 3-D effect of SMAs. In this model of a SMA strip, the shape memory effect is restricted to one-way applications, unless the SMA is coupled to an elastic structure which compels the SMA to recover the initial condition. The shape change of structure is caused by initial strained SMA strip bonded on the surface of host structure when thermally activated. The SMA strip starts transformation from the martensite to the austenite state upon actuation through heating, simultaneously recovering the initial strain, thus making host structure to change the shape. In the numerical results, a SMA strip actuator can generate enough recovery force to deform the host structure and sustain the deformed shape subjected to large external load, simultaneously.

NUMERICAL IMPLEMENTATION OF SHAPE MEMORY ALLOY CONSTITUTIVE EQUATIONS

Constitutive Model of SMAs

For the numerical analysis, the 3-D incremental formulation of the SMA constitutive model based on Lagoudas model (Qidwai and Lagoudas, 2000) is used to predict the thermomechanical responses of SMA. The model consists of three sets of equations: The constitutive equations, which describe the increment of strain, $\dot{\varepsilon}_{ij}$, in terms of the increments of stress, $\dot{\sigma}_{ij}$, temperature, $\dot{T}$, and martensite fraction, $\dot{\xi}$, i.e.,

$$\dot{\varepsilon}_{ij} = S_{ijkl}\,\dot{\sigma}_{kl} + \alpha_{ij}\dot{T} + Q_{ij}\,\dot{\xi} \tag{1}$$

Downloaded from jim.sagepub.com at KAIST GRADUATE SCHOOL OF MGMT on April 19, 2011

the transformation equations, which relate the increment of martensite fraction to transformation strain, $\dot{\varepsilon}^t_{ij}$, i.e.,

$$\dot{\varepsilon}^t_{ij} = \Lambda_{ij}\dot{\xi} \tag{2}$$

and the transformation surface equation, which controls the start of the forward and reverse phase transformation, i.e.,

$$\begin{aligned}\pi = {} & \sigma^{\text{eff}}_{ij}\Lambda_{ij} + \frac{1}{2}\sigma_{ij}\Delta S_{ijkl}\sigma_{kl} + \Delta\alpha_{ij}\sigma_{ij}(T - T_{\text{o}}) \\ & + \rho\Delta c\left[(T - T_{\text{o}}) - T\ln\left(\frac{T}{T_{\text{o}}}\right)\right] \\ & + \rho\Delta s_{\text{o}}T - \frac{\partial f}{\partial \xi} - \rho\Delta u_{\text{o}} = \pm Y^*\end{aligned} \tag{3}$$

where π is the thermodynamic force conjugated to ξ. The terms that are defined with the prefix Δ in Equation (3) indicate the difference of a quantity between the martensite and austenite phases as follows:

$$\begin{aligned}&\Delta S_{ijkl} = S^{\text{M}}_{ijkl} - S^{\text{A}}_{ijkl}, \quad \Delta\alpha_{ij} = \alpha^{\text{M}}_{ij} - \alpha^{\text{A}}_{ij}, \quad \Delta c = c^{\text{M}} - c^{\text{A}} \\ &\Delta s_{\text{o}} = s^{\text{M}}_{\text{o}} - s^{\text{A}}_{\text{o}}, \quad \Delta u_{\text{o}} = u^{\text{M}}_{\text{o}} - u^{\text{A}}_{\text{o}}\end{aligned} \tag{4}$$

Also, ρ, c, s_{o}, and u_{o} are the mass density, specific heat, specific entropy, and specific internal energy at the reference state, respectively. The superscript A stands for austenite phase, and superscript M stands for the martensite phase. The plus sign on the right hand side in Equation (3) should be used for the forward phase transformation (austenite to martensite), while the minus sign should be used for the reverse phase transformation (martensite to austenite). Note that the material constant Y^* is the measure of internal dissipation due to phase transformation and can be interpreted as the threshold value of the transformation surface π for the start of the phase transformation. The transformation function can be defined in terms of the transformation surface equation as follows:

$$\Phi = \begin{cases} \pi - Y^*, & \dot{\xi} > 0 \\ -\pi - Y^*, & \dot{\xi} < 0 \end{cases} \tag{5}$$

The transformation function Φ takes a similar role to the yield function in plasticity theory, but in this case, an additional constraint for martensite fraction ξ must also be satisfied. Constraints on the evolution of the martensite fraction are expressed as,

$$\begin{aligned}&\dot{\xi} \geq 0, \quad \Phi(\sigma, T, \xi) \leq 0, \quad \Phi\dot{\xi} = 0 \\ &\dot{\xi} \leq 0, \quad \Phi(\sigma, T, \xi) \leq 0, \quad \Phi\dot{\xi} = 0\end{aligned} \tag{6}$$

The inequality constraints on $\Phi(\sigma, T, \xi)$ is called as the transformation condition and regarded as a constraint on the state variables' admissibility. For $\Phi < 0$, Equation (6) requires $\dot{\xi} = 0$ and elastic response is obtained. On the other hand, the forward phase transformation (austenite to martensite) is characterized by $\Phi = 0$ and $\dot{\xi} > 0$, while the reverse phase transformation (martensite to austenite) is characterized by $\Phi = 0$ and $\dot{\xi} < 0$.

Finally, Equations (1), (2), and (6) can be composed for finding unknown state variables and predicting the thermomechanical responses of SMAs. In the formulation, Equation (1) is a generalized Hooke's law in incremental form, Equation (2) is the flow rule for transformation strain, and Equation (6) is the transformation function. In total, there are five unknown state variables in three Equations (1), (2), and (6), i.e., total strain tensor ε_{ij}, stress tensor σ_{ij}, transformation strain tensor ε^t_{ij}, temperature T, and martensite fraction ξ. If ε_{ij} and T are given, such as in finite element analysis, or σ_{ij} and T are given, when stress formulation is utilized, the other variables can be solved by using Newton–Raphson method and return mapping algorithms (Ortiz and Simo, 1986). In the above equations $S_{ijkl} = (C_{ijkl})^{-1}$ is the elastic compliance tensor and α_{ij} is the thermal expansion coefficient tensor, where both S_{ijkl} and α_{ij} are given in terms of the volume fraction of martensite by,

$$\begin{aligned}S_{ijkl} &= S^{\text{A}}_{ijkl} + \xi\left(S^{\text{M}}_{ijkl} - S^{\text{A}}_{ijkl}\right) \\ \alpha_{ij} &= \alpha^{\text{A}}_{ij} + \xi\left(\alpha^{\text{M}}_{ij} - \alpha^{\text{A}}_{ij}\right)\end{aligned} \tag{7}$$

where the superscripts A and M denote the austenite and martensite phases, respectively. The various other terms in Equations (1)–(6) are defined by,

$$Q_{ij} = \Delta S_{ijkl}\sigma_{kl} + \Delta\alpha_{ij}(T - T_{\text{o}}) + \Lambda_{ij} \tag{8}$$

where Λ_{ij} is the transformation tensor which determines the transformation strain direction and is assumed to have the following form:

$$\Lambda_{ij} = \begin{cases} \dfrac{3}{2}H\left(\bar{\sigma}^{\text{eff}}\right)^{-1}\bar{\sigma}^{\text{eff}'}_{ij}, & \dot{\xi} > 0 \\ H(\bar{\varepsilon}^{t-r})^{-1}\varepsilon^{t-r}_{ij}, & \dot{\xi} < 0 \end{cases} \tag{9}$$

where H is the maximum uniaxial transformation strain $\varepsilon^{t^{\max}}$, ε^{t-r} is the transformation strain at the reversal of phase transformation, and

$$\bar{\sigma}^{\text{eff}} = \sqrt{\frac{3}{2}\sigma^{\text{eff}'}_{ij}\sigma^{\text{eff}'}_{ij}}, \quad \sigma^{\text{eff}'}_{ij} = \sigma^{\text{eff}}_{ij} - \frac{1}{3}\sigma^{\text{eff}}_{kk}\delta_{ij}, \quad \bar{\varepsilon}^t = \sqrt{\frac{2}{3}\varepsilon^t_{ij}\varepsilon^t_{ij}} \tag{10}$$

where the effective stress $\sigma^{\text{eff}}_{ij} = \sigma_{ij} - \rho(\partial f/\partial\varepsilon^t_{ij})$ acts as a thermodynamic force conjugate to ε^t_{ij}. The hardening function $f(\xi)$ is responsible for the transformation-induced strain hardening in the SMA material and is given by,

$$f(\xi) = \begin{cases} \dfrac{1}{2}\rho b^{\text{M}}\xi^2 + (\mu_1 + \mu_2)\xi, & \dot{\xi} > 0 \\ \dfrac{1}{2}\rho b^{\text{A}}\xi^2 + (\mu_1 - \mu_2)\xi, & \dot{\xi} < 0 \end{cases} \tag{11}$$

Downloaded from jim.sagepub.com at KAIST GRADUATE SCHOOL OF MGMT on April 19, 2011

where ρb^{M}, ρb^{A}, μ_1, and μ_2 are transformation strain hardening material constants.

In the numerical implementing of the SMA constitutive model, the tangent stiffness tensor and the stress tensor at each integration point of all elements should be updated in each iteration for given increments of strain and temperature. To derive the tangent stiffness tensor, the consistency condition, $\dot{\Phi} = 0$, can be expressed by,

$$\frac{\partial \Phi}{\partial \sigma_{ij}}\dot{\sigma}_{ij} + \frac{\partial \Phi}{\partial T}\dot{T} + \frac{\partial \Phi}{\partial \xi}\dot{\xi} = 0 \tag{12}$$

Equations (1) and (12) can be used to eliminate $\dot{\xi}$ and obtain the relationship between stress increments and strain and temperature increments as,

$$\dot{\sigma}_{ij} = L_{ijkl}\dot{\varepsilon}_{kl} + l_{ij}\dot{T} \tag{13}$$

where the tangent stiffness tensor L_{ijkl} and tangent thermal moduli l_{ij} are defined by,

$$L_{ijkl} = \left(S_{ijkl} - \frac{Q_{ij}(\partial\Phi/\partial\sigma_{kl})}{(\partial\Phi/\partial\xi)}\right)^{-1},$$

$$l_{ij} = (S_{ijkl})^{-1}\left(Q_{kl}\frac{(\partial\Phi/\partial T) - (\partial\Phi/\partial\sigma_{ij})(S_{ijkl})^{-1}\alpha_{kl}}{(\partial\Phi/\partial\xi) - (\partial\Phi/\partial\sigma_{ij})(S_{ijkl})^{-1}Q_{kl}} - \alpha_{kl}\right) \tag{14}$$

Numerical Algorithms of SMA Constitutive Equations

To calculate the increment of stress for given strain and temperature increments, a return mapping integration algorithm (Ortiz and Simo, 1986) has been used. Equation (1) can be written in the following incremental form,

$$\Delta\sigma_{ij} = (S_{ijkl})^{-1}(\Delta\varepsilon_{kl} - \alpha_{kl}\Delta T - Q_{kl}\Delta\xi) \tag{15}$$

The elastic predictor is calculated in the first step by letting $\Delta\xi = 0$, i.e.,

$$\Delta\sigma_{ij}^{1} = (S_{ijkl})^{-1}(\Delta\varepsilon_{kl} - \alpha_{kl}\Delta T), \quad \sigma_{ij}^{1} = \sigma_{ij}^{0} + \Delta\sigma_{ij}^{1} \tag{16}$$

An iterative scheme is then applied to obtain the transformation corrector from Equation (15) by assuming $\Delta\varepsilon_{ij} = 0$, and $\Delta T = 0$, i.e., during the pth iteration,

$$\Delta\sigma_{ij}^{p+1} = -\left[S_{ijkl}(\xi^{p})\right]^{-1}Q_{kl}^{p}\Delta\xi^{p+1} \tag{17}$$

The transformation function, Equation (5), is expanded into a Taylor series about the current value of state variables, denoted by 'p', and is truncated at the linear part as shown below:

$$\Phi(\sigma_{ij},\xi) = \Phi^{p}(\sigma_{ij}^{p},\xi^{p}) + \frac{\partial\Phi^{p}}{\partial\sigma_{ij}}\Delta\sigma_{ij}^{p+1} + \frac{\partial\Phi^{p}}{\partial\xi}\Delta\xi^{p+1} \tag{18}$$

where temperature T is fixed, and thus $\Delta T^{p+1} = 0$. By using Equation (17), $\Delta\xi^{p+1}$ and $\Delta\varepsilon_{ij}^{t^{p+1}}$ can be obtained as follows:

$$\Delta\xi^{p+1} = \frac{\Phi^{p}}{(\partial\Phi^{p}/\partial\sigma_{ij})(S_{ijkl})^{-1}Q_{kl}^{p} - (\partial\Phi^{p}/\partial\xi)},$$
$$\Delta\varepsilon_{ij}^{t^{p+1}} = \Lambda_{ij}^{p}\Delta\xi^{p+1} \tag{19}$$

The state variables ξ^{p+1} and $\varepsilon_{ij}^{t^{p+1}}$ can then be updated as follows:

$$\xi^{p+1} = \xi^{p} + \Delta\xi^{p+1}, \quad \varepsilon_{ij}^{t^{p+1}} = \varepsilon_{ij}^{t^{p}} + \Delta\varepsilon_{ij}^{t^{p+1}} \tag{20}$$

and the stress can then be obtained by using the constitutive equation

$$\sigma_{ij}^{p+1} = \left[S_{ijkl}(\xi^{p+1})\right]^{-1}\left[\varepsilon_{kl} - \alpha_{kl}(\xi^{p+1})\Delta T - \left(\varepsilon_{kl}^{t^{p+1}}\right)\right] \tag{21}$$

The iterative procedure ends if $\Delta\xi^{p+1}$ is less than a specified tolerance (10^{-6}). If the convergence criterion is not satisfied, calculations given by Equations (17)–(21) are repeated until the convergence is achieved. The numerical algorithm of SMA constitutive equation for the ABAQUS user subroutine is illustrated in Figure 1. In the numerical algorithm, Newton–Raphson iteration method is used to solve the increment of martensite fraction in Equation (19).

FINITE ELEMENT MODELING

For the finite element modeling of SMA actuator and elastic structure, incompatible eight-node brick element is used (Figure 2). This type of element has been found to be suitable for 3-D stress analysis and improve the accuracy of bending stiffness. Thus, the interpolations of displacement fields (u_1, u_2, and u_3) in the x-y-z coordinate system for the eight-node brick element with incompatible modes are expressed as,

$$u_q = \sum_{i=1}^{8} N_i u_{qi} + \sum_{i=1}^{3} S_i a_{qi}, \quad q = 1,2,3 \tag{22}$$

where u_{qi} is the displacement of nodal point i, and a_{qi} are the variables of incompatible modes. The shape functions of the eight-node brick element, N_i ($i = 1$–8), and the shape functions of the incompatible modes S_i ($i = 1$–3), are

$$N_1 = \frac{(1-r)(1-s)(1-t)}{8}, \quad N_2 = \frac{(1+r)(1-s)(1-t)}{8}$$
$$N_3 = \frac{(1+r)(1+s)(1-t)}{8}, \quad N_4 = \frac{(1-r)(1+s)(1-t)}{8}$$
$$N_5 = \frac{(1-r)(1-s)(1+t)}{8}, \quad N_6 = \frac{(1+r)(1-s)(1+t)}{8}$$
$$N_7 = \frac{(1+r)(1+s)(1+t)}{8}, \quad N_8 = \frac{(1-r)(1+s)(1+t)}{8}$$
$$S_1 = (1-r^2), \quad S_2 = (1-s^2), \quad S_3 = (1-t^2) \tag{23}$$

Downloaded from jim.sagepub.com at KAIST GRADUATE SCHOOL OF MGMT on April 19, 2011

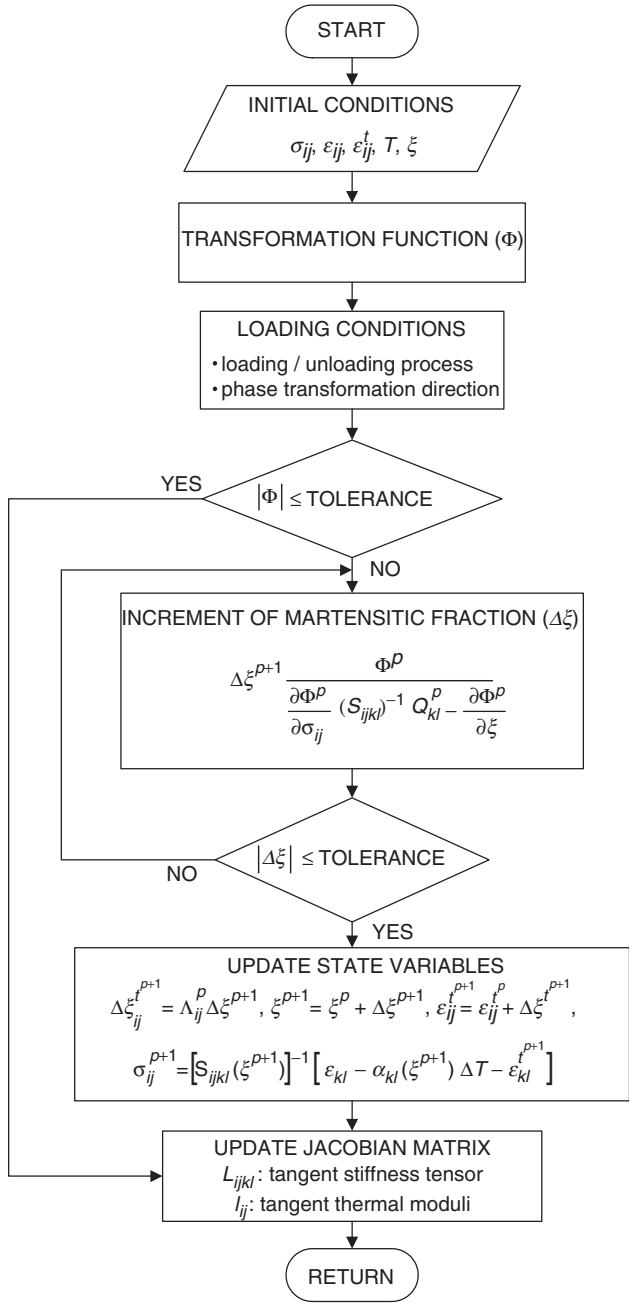

Figure 1. *Algorithm of the SMA constitutive equation for the ABAQUS user subroutine.*

where r, s, and t are the natural coordinates for each element whose values vary form -1 to $+1$. To consider the large displacements, large strains, and material nonlinear of SMAs, the Green–Lagrange strain–displacement relationships are adopted in this analysis. The strain vector in material Cartesian coordinates can be written as follows:

$$\varepsilon_{xx} = u_{1,1} + \frac{1}{2}\left[(u_{1,1})^2 + (u_{2,1})^2 + (u_{3,1})^2\right]$$
$$\varepsilon_{yy} = u_{2,2} + \frac{1}{2}\left[(u_{1,2})^2 + (u_{2,2})^2 + (u_{3,2})^2\right]$$

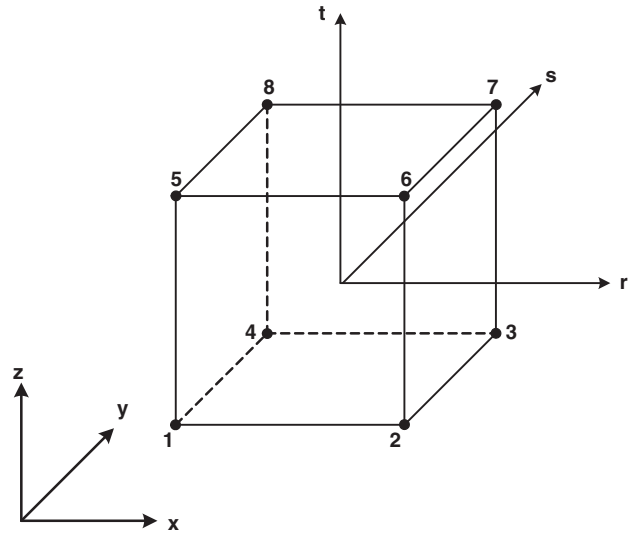

Figure 2. *Schematic of the eight-node element.*

$$\varepsilon_{zz} = u_{3,3} + \frac{1}{2}\left[(u_{1,3})^2 + (u_{2,3})^2 + (u_{3,3})^2\right]$$
$$\varepsilon_{xy} = \frac{1}{2}(u_{1,2} + u_{2,1}) + \frac{1}{2}(u_{1,1}u_{1,2} + u_{2,1}u_{2,2} + u_{3,1}u_{3,2})$$
$$\varepsilon_{yz} = \frac{1}{2}(u_{2,3} + u_{3,2}) + \frac{1}{2}(u_{1,2}u_{1,3} + u_{2,2}u_{2,3} + u_{3,2}u_{3,3})$$
$$\varepsilon_{xz} = \frac{1}{2}(u_{1,3} + u_{3,1}) + \frac{1}{2}(u_{1,1}u_{1,3} + u_{2,1}u_{2,3} + u_{3,1}u_{3,3}) \tag{24}$$

where u_1, u_2, u_3 are the displacements and the comma denotes the partial differentiation.

Considering the nonlinear motion of a body in a Cartesian coordinate system, the equilibrium position of the body is evaluated at the discrete time position 0, Δt, $2\Delta t$, $3\Delta t$, ..., where Δt is an increment in time. Assume that the solution for the static variables for all time steps from time 0 to time t have been solved and the solution for time $t + \Delta t$ is required next. It is noted that the solution process for the next required equilibrium position is typical and would be applied repeatedly until the complete solution path has been solved. By using the principle of virtual displacement, the equilibrium of the body in the configuration at time $t + \Delta t$ can be expressed. The principle of virtual displacement requires that

$$\int_{t+\Delta t V} {}^{t+\Delta t}\tau_{ij}\delta_{t+\Delta t}e_{ij}\,{}^{t+\Delta t}\mathrm{d}v = {}^{t+\Delta t}R \tag{25}$$

where ${}^{t+\Delta t}R$ is the external virtual work expression,

$${}^{t+\Delta t}R = \int_{t+\Delta t A} {}^{t+t\Delta t}_{t+t\Delta t}t_k\,\delta u_k\,{}^{t+\Delta t}\mathrm{d}a + \int_{t+\Delta t V} {}^{t+\Delta t}\rho^{t+\Delta t}_{t+\Delta t}f_k\delta u_k\,{}^{t+\Delta t}\mathrm{d}v \tag{26}$$

Downloaded from jim.sagepub.com at KAIST GRADUATE SCHOOL OF MGMT on April 19, 2011

In Equations (25) and (26), δu_k is a virtual variation in the current displacement components ${}^{t+\Delta t}u_k$, and $\delta_{t+\Delta t}e_{ij}$ are the corresponding virtual variations in strain. The Cauchy stress tensor is denoted by ${}^{t+\Delta t}\tau_{ij}$ at time $t+\Delta t$ and ${}^{t+\Delta t}_{t+\Delta t}t_k$, ${}^{t+\Delta t}\rho$, and ${}^{t+\Delta t}_{t+\Delta t}f_k$ represent the surface force, the specific mass and the body force per unit mass at time $t+\Delta t$, respectively. By using the Lagrangian formulation (Hibbitt et al. 1970), the approximate equilibrium equation can be solved. Using Equations (22) and (24) to evaluate the displacement derivatives required in the integrals, Equations (25) and (26) becomes, considering a single element

$$\left({}^{t}_{t}\mathbf{K}_{\mathrm{L}} + {}^{t}_{t}\mathbf{K}_{\mathrm{NL}}\right)\mathbf{u} = {}^{t+\Delta t}\mathbf{R} - {}^{t}_{t}\mathbf{F} \tag{27}$$

where ${}^{t}_{t}\mathbf{K}_{\mathrm{L}}$, ${}^{t}_{t}\mathbf{K}_{\mathrm{NL}}$ and ${}^{t}_{t}\mathbf{F}$ are obtained from the finite element evaluation, respectively, i.e.,

$${}^{t}_{t}\mathbf{K}_{\mathrm{L}} = \int_{{}^{t}V} {}^{t}_{t}\mathbf{B}^{T}_{\mathrm{L}}\, {}^{t}\mathbf{C}\, {}^{t}_{t}\mathbf{B}_{\mathrm{L}}\, {}^{t}\, \mathrm{d}v \tag{28}$$

$${}^{t}_{t}\mathbf{K}_{\mathrm{NL}} = \int_{{}^{t}V} {}^{t}_{t}\mathbf{B}^{T}_{\mathrm{NL}}\, {}^{t}\tau\, {}^{t}_{t}\mathbf{B}_{\mathrm{NL}}\, {}^{t}\, \mathrm{d}v \tag{29}$$

$${}^{t}_{t}\mathbf{F} = \int_{{}^{t}V} {}^{t}_{t}\mathbf{B}^{T}_{\mathrm{L}}\, {}^{t}\hat{\tau}\, \mathrm{d}v \tag{30}$$

In Equations (28)–(30), the elements of the linear and nonlinear strain-displacement transformation matrices ${}^{t}_{t}\mathbf{B}_{\mathrm{L}}$ and ${}^{t}_{t}\mathbf{B}_{\mathrm{NL}}$, respectively, and the elements of the incremental material property matrix, ${}_{t}\mathbf{C}$, are defined with respect to the configuration at time t, ${}^{t}\tau$ is a matrix and ${}^{t}\hat{\tau}$ is a vector of Cauchy stresses in the configuration at time t. The loading vector ${}^{t+\Delta t}\mathbf{R}$ in Equation (27) can be obtained from the usual finite element evaluation way and detailed expressions for the parameters used in Equations (27)–(30) can be found in Bathe et al. (1975).

RESULTS AND DISCUSSION

For the numerical results presented in this article, the ABAQUS finite element program has been utilized with an appropriate user supplied subroutine (UMAT) for the modeling SMA and elastic structures. The material properties of SMA (Qidwai and Lagoudas, 2000) used in the finite element analysis are given in the Table 1.

Code Verification and Comparison

To verify present numerical algorithm developed for the thermomechanical responses of SMA strip actuators, the simple cases are investigated and the result is compared with Qidwai and Lagoudas (2000) result. Figure 3 shows the schematic of the SMA model and the loading histories. Only two 3-D incompatible eight-node elements are used in this model. Because the use of UMAT generally requires considerable development and testing, initial testing on a simple element model is recommended. In the case of Qidwai and Lagoudas (2000), it is assumed that the boundary conditions are such that except for the axial component of stress σ_{xx}, the rest of the stresses are zero. But this boundary condition makes 3-D model of SMAs be reduced to 1-D model. So, it is not appropriate to consider thermomechanical characteristics of 3-D SMAs. In the present numerical results, two kinds of boundary conditions are considered such as (i) case I: the rest of the stresses are

Table 1. Material parameters of SMAs.

Material constants	Values	Model variables
E^{A}	70.0×10^{9} Pa	Used to calculate isotropic compliance tensor, S^{A} and S^{M}
E^{M}	30.0×10^{9} Pa	
$\nu^{\mathrm{A}}=\nu^{\mathrm{M}}$	0.3	
α^{A}	22.0×10^{-6}/K	Used to calculate isotropic thermal expansion coefficient tensor, α^{A} and α^{M}
α^{M}	10.0×10^{-6}/K	
$\rho\Delta c = c^{\mathrm{M}} - c^{\mathrm{A}}$	0.0 J/(m^{3}K)	
H	0.05	$\dfrac{\rho\Delta s_{\mathrm{o}}}{H} = -\left(\dfrac{\mathrm{d}\sigma}{\mathrm{d}T}\right)^{\mathrm{A}}$
$\left(\dfrac{\mathrm{d}\sigma}{\mathrm{d}T}\right)^{\mathrm{A}} = \left(\dfrac{\mathrm{d}\sigma}{\mathrm{d}T}\right)^{\mathrm{M}}$	70.0×10^{6} Pa/K	
A^{of}	315.0 K	$\gamma = \rho\Delta u_{\mathrm{o}} + \mu_1 = \dfrac{1}{2}\rho\Delta s_{\mathrm{o}}(M^{\mathrm{os}} + A^{\mathrm{of}})$
A^{os}	295.0 K	$\rho b^{\mathrm{A}} = -\rho\Delta s_{\mathrm{o}}(A^{\mathrm{of}} - A^{\mathrm{os}})$
A^{os}	291.0 K	$\mu_2 = \dfrac{1}{4}(\rho b^{\mathrm{A}} - \rho b^{\mathrm{M}})$
M^{of}	271.0 K	$Y^{*} = -\dfrac{1}{2}\rho\Delta s_{\mathrm{o}}(A^{\mathrm{of}} - M^{\mathrm{os}}) + \dfrac{1}{4}\rho\Delta s_{\mathrm{o}}(M^{\mathrm{os}} - M^{\mathrm{of}} - A^{\mathrm{of}} + A^{\mathrm{os}})$

Downloaded from jim.sagepub.com at KAIST GRADUATE SCHOOL OF MGMT on April 19, 2011

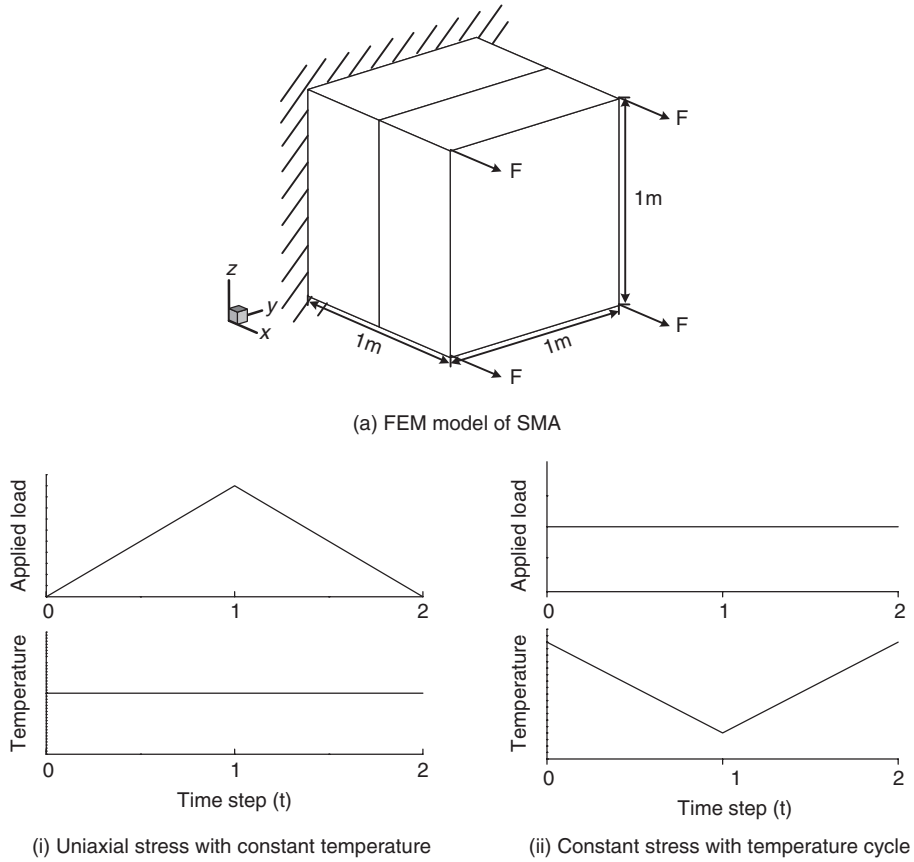

(a) FEM model of SMA

(i) Uniaxial stress with constant temperature (ii) Constant stress with temperature cycle

(b) Loading histories

Figure 3. *FEM model and loading histories.*

zero except for the axial component of stress σ_{xx}, and (ii) case II: cantilevered ($u = v = w = 0$, at $X = 0$). Firstly, the uniaxial stress with constant temperature loading case is investigated. The initial temperature is chosen to be austenite finish temperature, $T = 42°C$. The isothermal loading history is applied and assumed to be a linear function of time step, t. The maximum load is applied such that all austenite phases transform to martensite and transformation strain of 5% is followed by full unloading to austenite state. In Figure 4, the axial stress is plotted against the axial strain. As can be seen, the present result with boundary condition (case I) is good comparable with Qidwai and Lagoudas (2000). But in case of cantilevered boundary condition (case II), there are some differences in phase transformation region, because the phenomenon of stress concentration occurs in the boundary region. It should be expected that the result of case II should be same with Lagoudas if the number of elements are increased and observing point is far enough from boundary area to ignore the effect of stress concentration. Lastly, uniaxial constant stress thermally induced transformation is investigated. The constant stress with temperature cycle loading is applied. The SMA is put through a temperature cycle at a constant axial stress of 50 MPa. The initial temperature of the SMA is above A^{of}. Next the

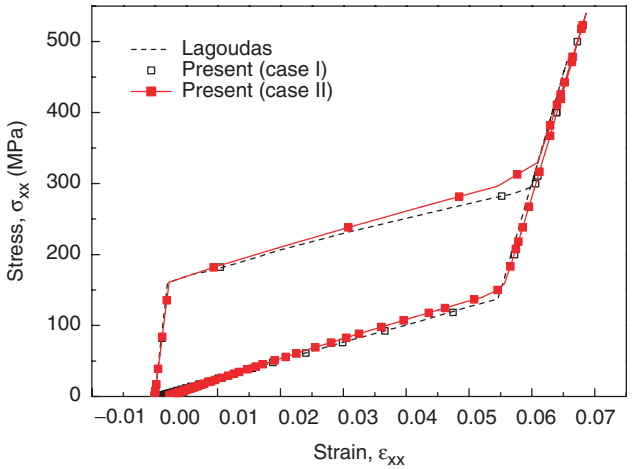

Figure 4. *Hysteresis of axial stress vs axial strain.*

temperature is decreased below M^{of} for full forward transformation and the increased above A^{of} again for full reverse transformation. In Figure 5, the uniaxial strain with temperature cycle is illustrated. As can be seen, both present results (case I and II) are well compatible with Lagoudas results. But in case of cantilevered boundary condition, thermally induced transformation strain is little more than 0.05. If the

Downloaded from jim.sagepub.com at KAIST GRADUATE SCHOOL OF MGMT on April 19, 2011

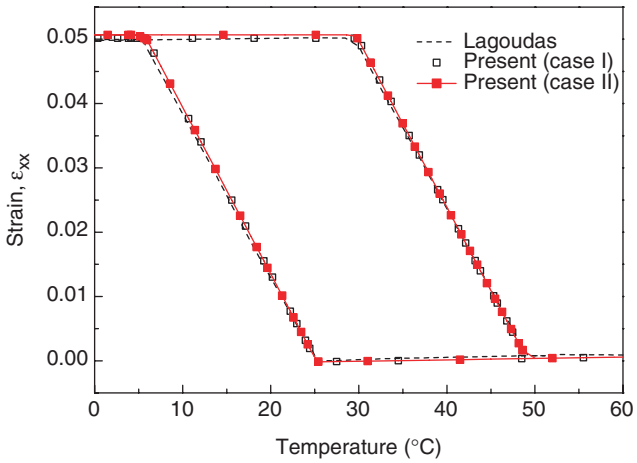

Figure 5. *Hysteresis of axial strain curve with temperature cycle.*

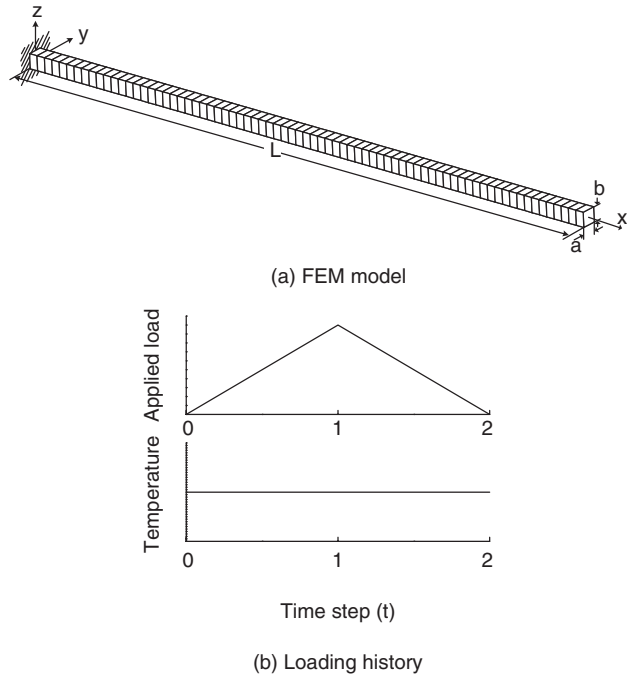

Figure 6. *FEM model of a SMA wire and loading history.*

SMA is subjected to only uniaxial stress, the strain cannot exceed the value of 0.05. But the stress concentration effect induced cantilevered boundary condition generates complex stress condition near the boundary area.

Thermomechanical Responses of SMA Wire and Strip Actuator

SMA wire and strip are modeled numerically to investigate the thermomechanical responses and capabilities of SMAs as actuators. First, the SMA wire is investigated and this numerical result is compared with 1-D SMA models such as Liang (1990) and Brinson (1993). Figure 6 illustrates the SMA wire model with seventy-five 3-D incompatible eight-node elements

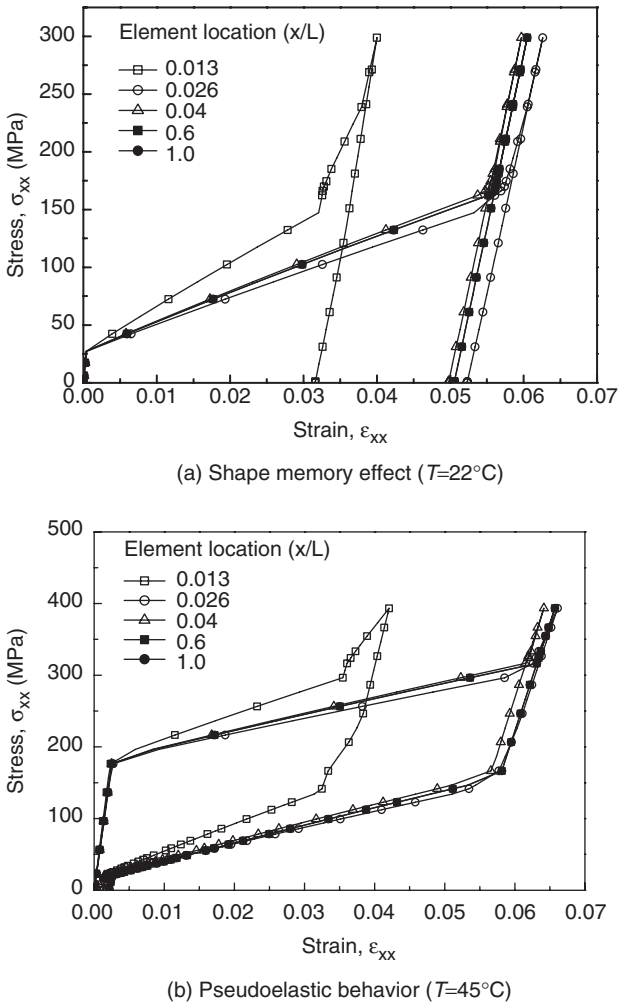

Figure 7. *Stress–strain curves with different temperature.*

in x-direction and loading history. This wire model has a rectangular cross section ($a = b = 0.4$ mm) and its dimension is very small comparing with longitudinal dimension ($L/a = 75$). Figure 7 shows the stress and strain curves at the different location of wire elements with temperature $T = 22$ and 45°C indicating the shape memory effect and pseudoelastic behavior, respectively. As can be seen, stress and strain curves have the different values with respect to the different location due to the stress concentration near the boundary area even if simply uniaxial load is applied. In case of shape memory effect, the residual transformation strain cannot exceed the value of 0.05 in this model if a SMA is subjected to uniaxial stress. But the effect of stress concentration induced cantilevered boundary condition induces the complex stress condition near boundary area even if simply uniaxial load is applied (Figure 8). So, transformation strain at the element location $x/L = 0.026$ should be beyond the limited value of 0.05. When the element location is far enough from boundary condition, the effect of stress concentration can be neglected such as $x/L = 0.6$ and $x/L = 1.0$

Downloaded from jim.sagepub.com at KAIST GRADUATE SCHOOL OF MGMT on April 19, 2011

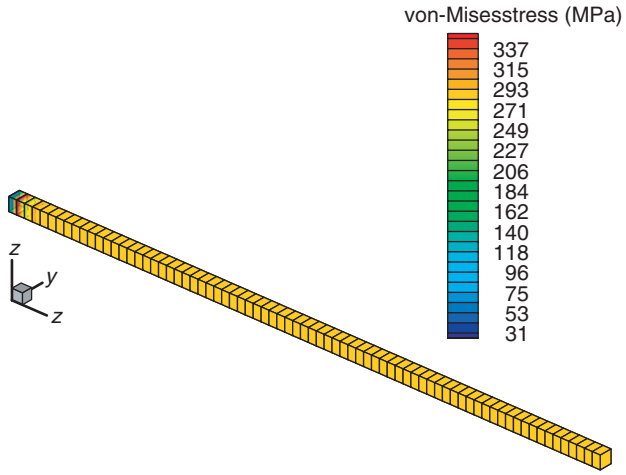

Figure 8. *Stress distribution of a SMA wire at time step $t=1$ and $T=22^{\circ}C$.*

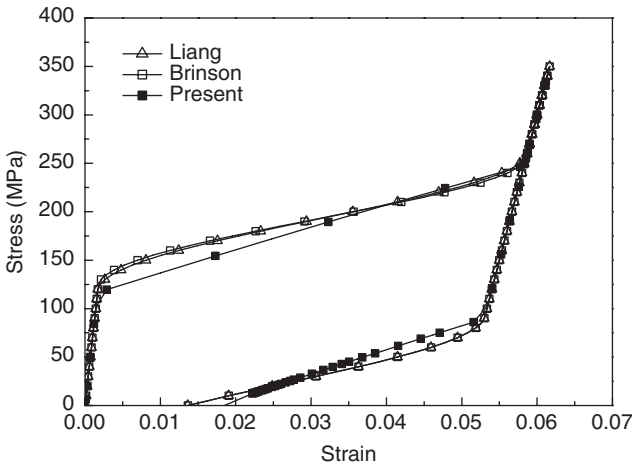

Figure 9. *Stress–strain curves at temperature, $T=35^{\circ}C$.*

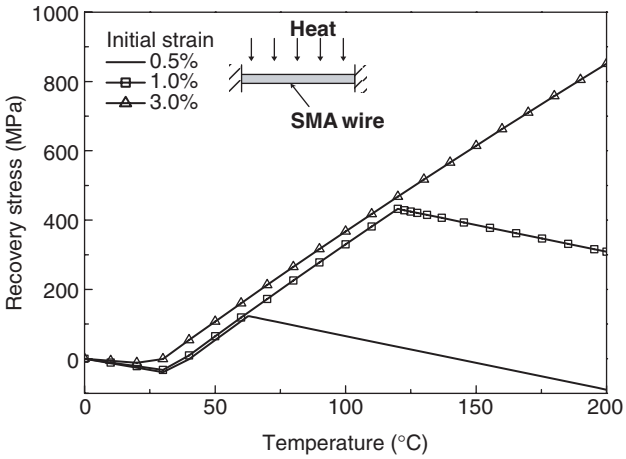

Figure 10. *Recovery stress of a SMA wire vs temperature.*

and the transformation strains are within the value of 0.05. But, if the SMA wire is modeled based on 1-D constitutive equation, this model cannot predict such a phenomenon and illustrates the same value of stress–strain curves at all locations. So, the development of SMA constitutive equation based on 3-D model is necessary to investigate the thermomechanical response of SMA with more accuracy. Uniaxial stress–strain curves with temperature $T=35^{\circ}C$ predicted by the different equations are plotted in Figure 9. Present result at the location $x/L=1$ is compared with Liang (1990) and Brinson (1993) equations which are implemented numerically based on 1-D constitutive equation. To modify the stress of phase transformation start, critical stresses for transformation are used in the Brinson model as follows:

$$\sigma_s^{cr}=5\ \text{MPa},\quad \sigma_f^{cr}=136\ \text{MPa} \tag{31}$$

As can be seen, the stress–strain curves of all three are similar, and they give the same amount of total hysteresis in a complete loading–unloading cycle, except for the curve where the phase of the SMA is transformed. Liang (1990) and Brinson (1993) equations are based on cosine hardening law but present model is based on polynomial hardening law. To illustrate the capability of the SMA wire as an actuator, the recovery stress induced by heating with different initial strains is investigated. The SMA wire which has residual initial strain generates extremely large recovery stress as the temperature is raised through austenite start temperature, and austenite finish temperature, because both edges of the SMA wire is clamped as the transformation occurs. As can be seen from Figure 10, the recovery stress is decreased until A^{os} (22°C) due to thermal expansion effect. Although the temperature is above A^{os}, the recovery stress continues to decrease except in the case of 3% initial strain, because thermal expansion is more influential than recovery stress when SMA is subjected to low initial strain. After the end of phase transformation induced temperature, the recovery stress is decreased again due to thermal expansion effect. It can be observed that larger recovery stress and higher modified austenite finish temperature should be induced by increasing the initial strain.

For the next numerical analysis, a SMA strip model with cantilever subjected to uniaxial force is illustrated in Figure 11. This analysis uses $16\times10\times1$ mesh with 3-D incompatible eight-node elements. Figure 12 shows the unique characteristics of the SMA strip at different temperatures such as shape memory effect and pseudoelastic behavior observed at $x/a=1$ and $y/b=0.5$ respectively. The hysteresis loop of recovery stress with respect to temperature variation is illustrated in Figure 13. The SMA strip is restrained during the phased transformation induced by heating process, so that the large recovery stress is generated by shape memory effect. The recovery stress is decreased until A^{os} (22°C) due to thermal expansion effect. But in case of 1% initial strain, the recovery stress continues to decrease after the temperature of A^{os}. Because the stress

Downloaded from jim.sagepub.com at KAIST GRADUATE SCHOOL OF MGMT on April 19, 2011

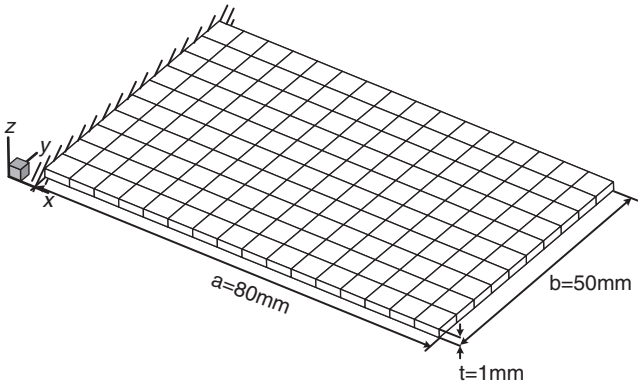

Figure 11. *FEM model of a SMA strip.*

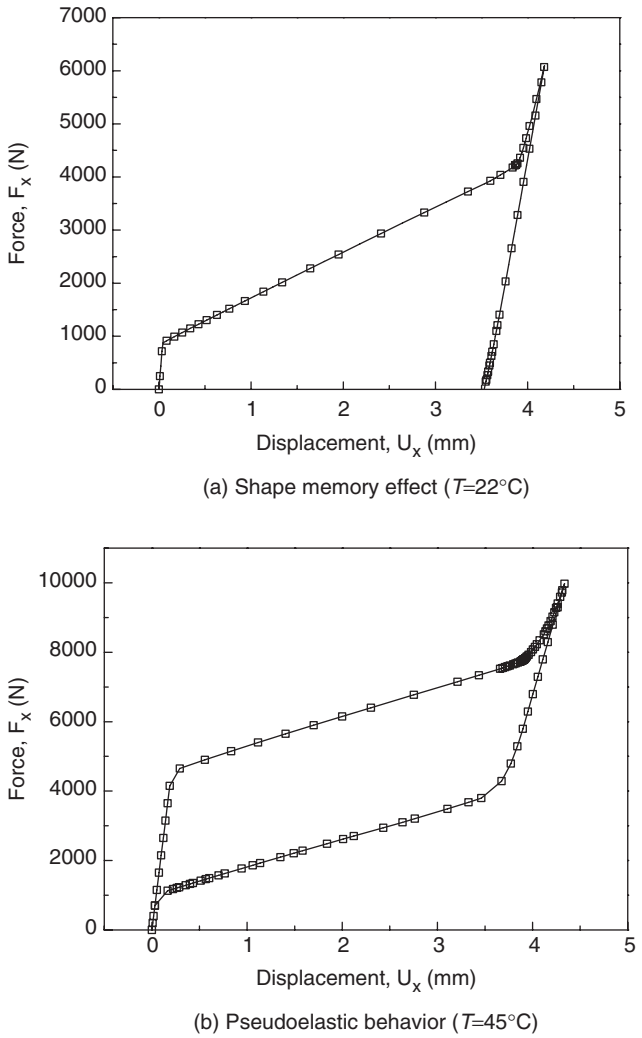

Figure 12. *Unique characteristics of a SMA strip with different temperatures.*

generated by thermal expansion is more influential than recovery stress induced by phase transformation. After austenite finish temperature is modified by initial strain, the recovery stress should be decreased again due to thermal expansion effect.

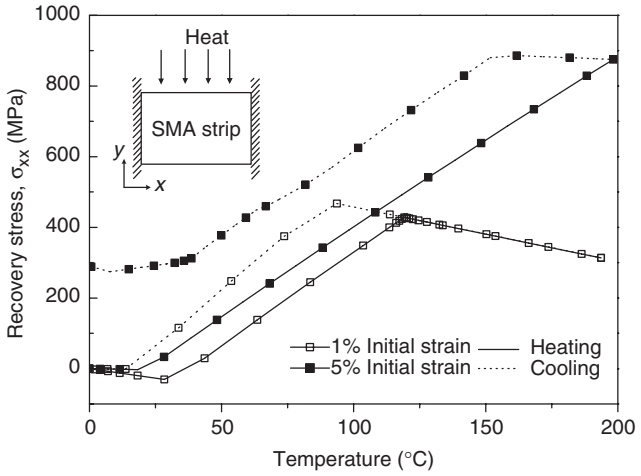

Figure 13. *Hysteresis of recovery stress vs temperature cycle.*

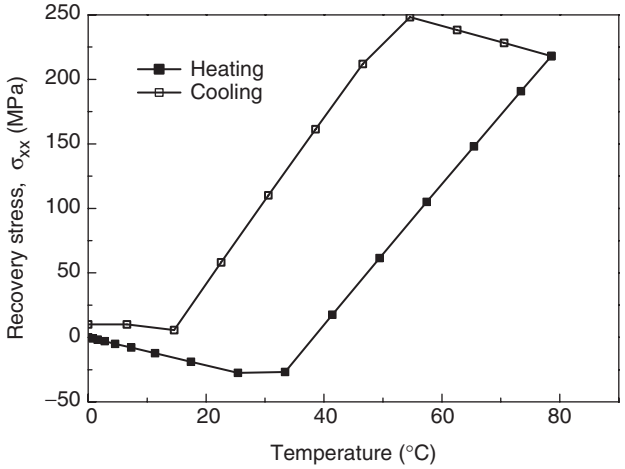

Figure 14. *Residual recovery stress with 1% initial strain by temperature cycle.*

As can be seen from this hysteresis loop, recovery stress is returned to the initial state in case of 1% initial strain except in case of 5% initial strain. In case of 1% initial strain, reverse phase transformation to austenite is completely finished by heating process. So complete forward phase transformation can be acquired by cooling process. But in case of 5% initial strain, reverse phase transformation to austenite does not get completed. Because the initial state at the beginning of cooling process is not a complete austenite phase, residual recovery stress remains at the end of cooling process. As should be expected, the recovery stress with 1% initial strain cannot be returned to initial state when reverse phase transformation is not completed by heating process (Figure 14). The distribution of residual recovery stress of the SMA strip with 5% initial strain is illustrated in Figure 15. In case of 5% initial strain, the distributions of martensite fraction at various temperatures are also investigated. Figure 16 illustrates the martensite fraction of the SMA strip at $T = 200°C$ and

Downloaded from jim.sagepub.com at KAIST GRADUATE SCHOOL OF MGMT on April 19, 2011

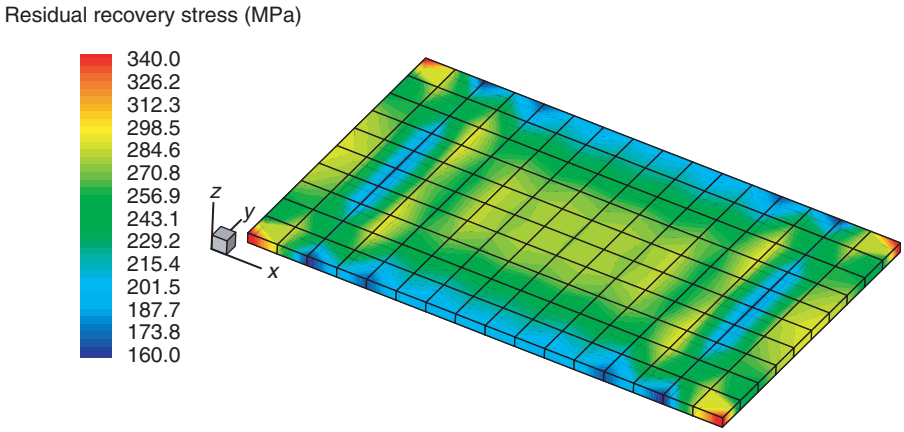

Figure 15. *Residual recovery stress (σ_{xx}) on a SMA strip with 5% initial strain.*

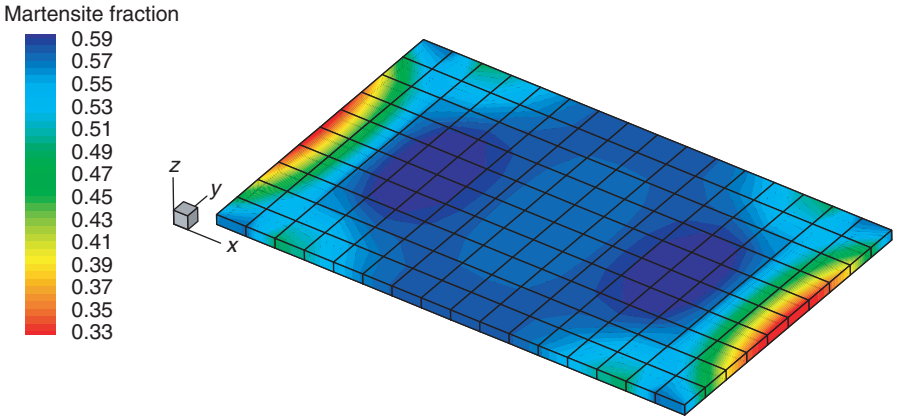

(a) Martensite fraction on a SMA strip (T=200°C)

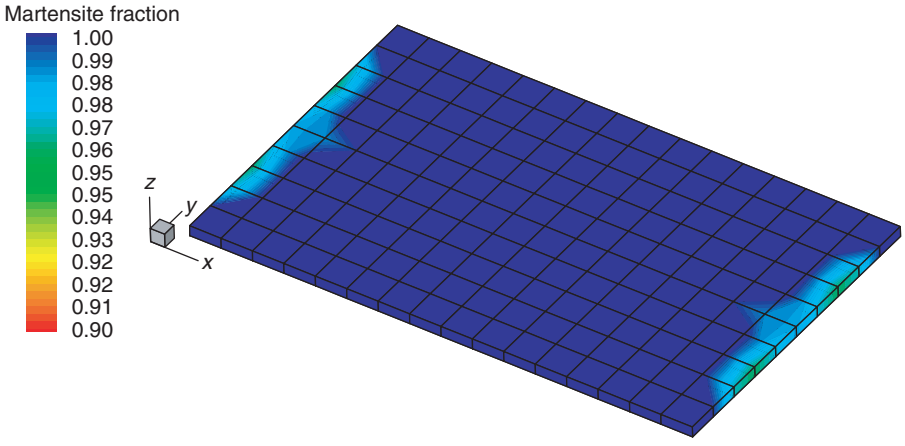

(b) Martensite fraction on a SMA strip (T=0°C)

Figure 16. *Distribution of martensite fraction with different temperature (5% initial strain).*

at the end of the temperature cycle, $T = 0°C$. The numerical results show that the SMA strip does not recover the initial martensite fraction and generates the residual recovery stress at the end of the temperature cycle. These phenomena should cause the SMA strip to be an irreversible actuator, even if SMA is coupled to an elastic structure which compels SMA to recover the initial condition. Therefore, the research about the

Downloaded from jim.sagepub.com at KAIST GRADUATE SCHOOL OF MGMT on April 19, 2011

interactions between host structure and the SMA strip is necessary to design reversible shape adaptive structures.

Applications of SMA Strip Actuator to Elastic Structures

In this section, the interactions between the SMA strip actuator and the elastic structure are investigated. The SMA strip actuator coupled with elastic structure can be used to generate bending force and for the shape modification. The host elastic structure is made of aluminum, the properties of which are as follows:

$$E = 69\,\text{GPa}, \quad v = 0.33, \quad \alpha = 23.6 \times 10^{-6}/^{\circ}\text{C} \quad (32)$$

For the numerical analysis, following assumptions are considered: (i) the SMA strip is perfectly bonded with aluminum by using epoxy adhesive, (ii) the SMA strip actuator is activated by electrically heating, and (iii) the SMA strip is thermally insulated from the rest of aluminum. The constrained condition such as tie is applied between the surface of the SMA strip and host structure. So two surfaces of the SMA strip and host structure are tied together in the simulation. The surface of the SMA strip is defined as the master surface and that of host structure is done as the slave surface. The master nodes are calculated and used to determine the slave nodes according to constrained condition.

The first numerical example is a beam structure coupled with the SMA strip for generating bending force (Figure 17). Aluminum beam and the SMA strip are respectively modeled by $10 \times 2 \times 1$ mesh using 3-D eight-node elements with cantilevered boundary condition. The SMA strip is subjected to initial strain in x-direction. When the SMA strip is activated by raising its temperature above the austenite start temperature, strain recovered in the activated SMA strip causes bending deformation due to the off-center placement of the SMA strip. Figure 18 shows the vertical tip deflection with temperature variation for the various initial strains. One can get the larger vertical deflection of host structure by increasing the initial strain of the SMA strip. The deflection of structure with 5% initial strain occurs at lower temperature than with other initial strain cases, because larger recovery stress should be generated by increasing the initial strain of the SMA strip (Figures 10 and 13). In the case of 1.0% initial strain, vertical deflection remains constant over the temperature $T = 130^{\circ}\text{C}$, due to the complete phase transformation to austenite state over this temperature. Also, the SMA strip actuator effect on the shape control is investigated. The elastic beam with 3.0% initial strain of the SMA strip is originally flat and then is exposed to an uniform distributed load of 300,000 N/m^2. Figure 19 shows the calculated deflection of the beam under different input incremental temperature. In this numerical results, the SMA strip actuator can generate enough recovery force to bend the host structure, also sustain its shape against large external uniform load. To design a reversible shape adaptive structure with SMAs, the interactions between the SMA strip and elastic structure

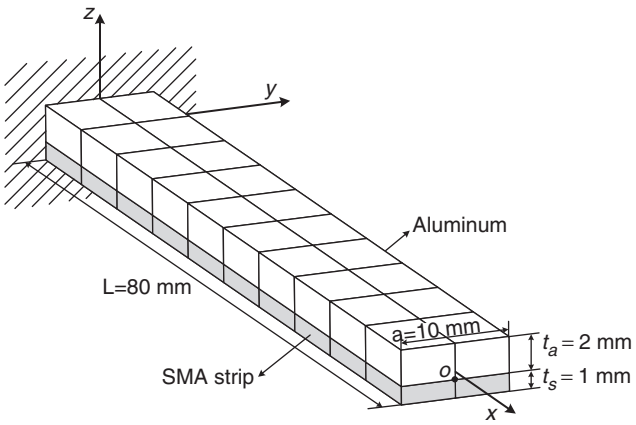

Figure 17. *FEM model of the beam structure with a SMA strip.*

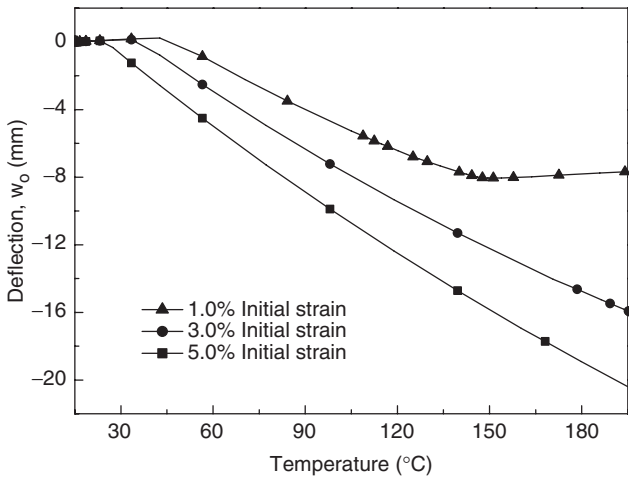

Figure 18. *Vertical tip deflection vs temperature variation.*

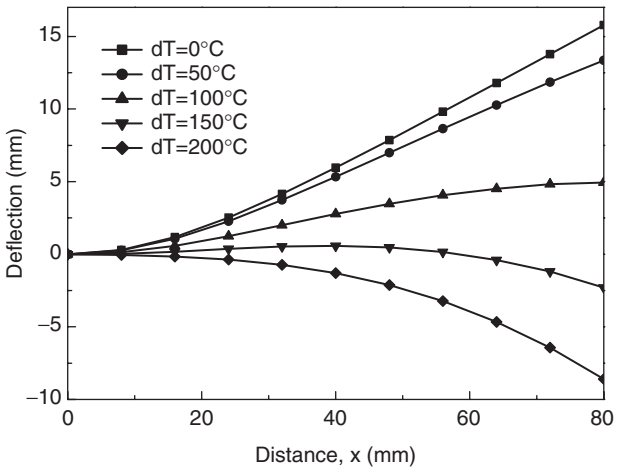

Figure 19. *The deflection under uniform load and different temperature increment.*

Downloaded from jim.sagepub.com at KAIST GRADUATE SCHOOL OF MGMT on April 19, 2011

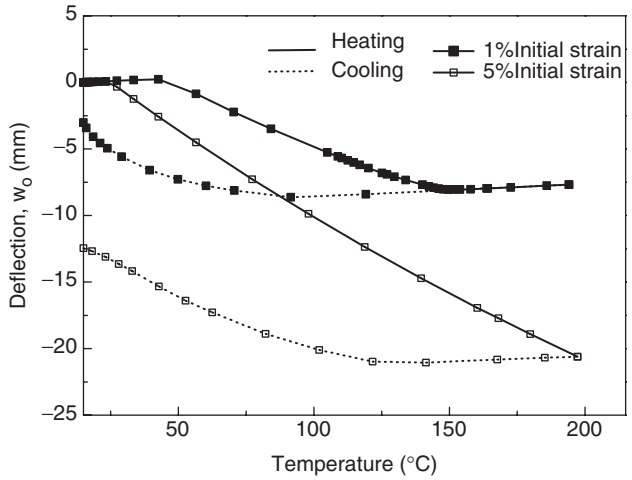

Figure 20. *Vertical deflection vs temperature cycle on a SMA strip.*

with temperature cycle on the SMA strip should be investigated. Figure 20 shows the hysteresis of deflection versus temperature cycle on the SMA strip with 1 and 5% initial strains, where the deformed shape cannot be fully recovered at the end of cycle. To investigate internal condition of the SMA strip at the end of temperature cycle, the residual recovery stress and distribution of martensite fraction with 1 and 5% initial strains is illustrated in Figures 21 and 22, respectively. The recovery stress of the SMA strip does not decrease to zero, even if the SMA strip is coupled with elastic structure. In case of 1% initial strain, it can be found that the value of martensite fraction exceeds the initial value of 0.2 in some areas. So, there should be a limitation to make a reversible shape adaptive structure using one-way shape memory alloys and the investigation of the interactions between host structure and the SMA actuator is necessary to make a more accurate structural actuator.

The next numerical model is a conical shell structure which can be applied to the variable-area fan nozzle (VAFN). The object of the VAFN structure is to decrease jet noise during takeoff and reduce drag by changing the area of inlet or outlet fan nozzle. Figure 23 shows the numerical model of conical shell structure with a SMA strip. The conical shell structure consists of aluminum and a SMA strip layer and each layer is modeled using $20 \times 10 \times 1$ mesh with 3-D eight-node elements. The SMA strip is subjected to initial strain in axial direction and bonded on the surface of host structure. Boundary condition is cantilevered and each geometric dimensions are aluminum thickness $(t_a) = 2\,\text{mm}$, SMA strip thickness $(t_s) = 0.5\,\text{mm}$, length (L) $= 150\,\text{mm}$, shallow angle $(\phi) = 30°$, and radius $(R_a) = 100\,\text{mm}$ and $(R_b) = 50\,\text{mm}$. Figure 24 shows the hysteresis of tip deflection versus temperature cycle on the SMA strip with 3 and 5% initial strain. In this numerical simulation, a SMA strip can generate enough force to deform host structure to desired shape but

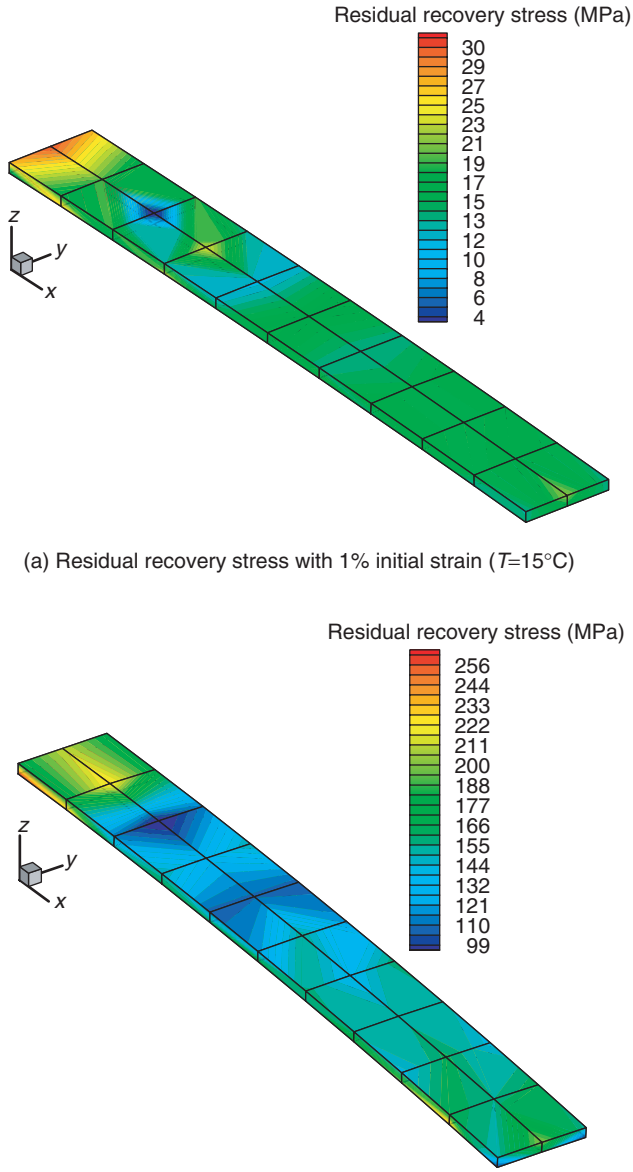

(a) Residual recovery stress with 1% initial strain (T=15°C)

(b) Residual recovery stress with 5% initial strain (T=15°C)

Figure 21. *Distribution of residual recovery stress at the end of temperature cycle.*

deformed shape does not get recovered to its initial shape at the end of cycle. To investigate the SMA strip internal conditions at the end of temperature cycle, the recovery stress and martensite fraction is illustrated. Figure 25 shows the distribution of residual recovery stresses in case of 3 and 5% initial strain of the SMA strip. As can be seen, recovery stress of the SMA strip does not decrease to zero at the end of temperature cycle. This residual recovery stress of the SMA strip causes the host structure to remain as a deformed shape. Also, the martensite fraction of the SMA strip at the end of cycle is illustrated in Figure 26. In the case of 3% initial strain, the martensite fraction of the SMA strip does not recover its original value of 0.6, but 5% initial strain, the distribution of martensite fraction almost

Downloaded from jim.sagepub.com at KAIST GRADUATE SCHOOL OF MGMT on April 19, 2011

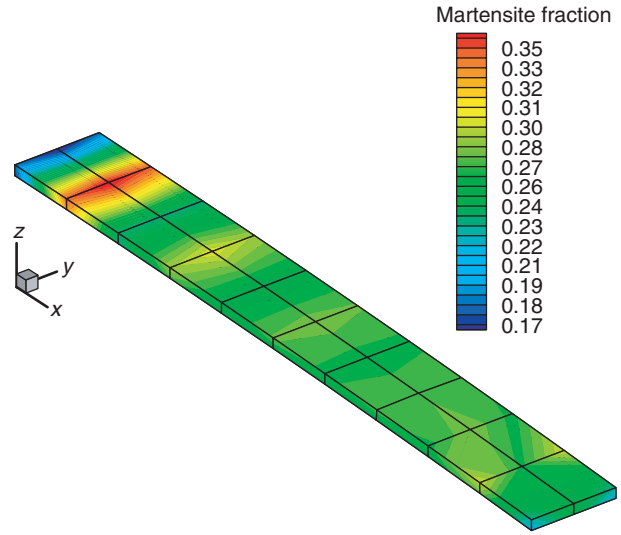

(a) Martensite fraction with 1% initial strain (T=15°C)

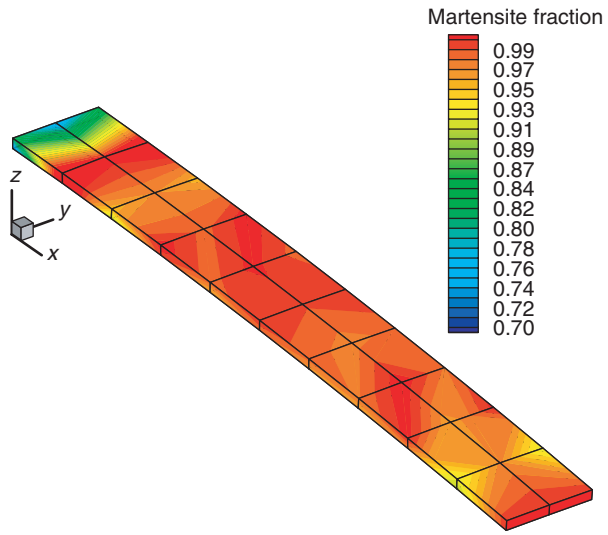

(b) Martensite fraction with 5% initial strain (T=15°C)

Figure 22. *Distribution of martensite fraction of SMA strip at the end of temperature cycle.*

recovers its initial value of 1.0, except near the boundary area. In this numerical analysis, residual recovery stress of the SMA strip causes host structure to remain in deformed shape and martensite fraction of the SMA strip not to recover its initial value. Therefore, it is difficult to design a perfect reversible shape adaptive structure using this one-way SMA strip, even if the strip is coupled with elastic structure.

CONCLUSIONS

The thermomechanical responses of SMA actuators and their applications in the shape adaptive structures

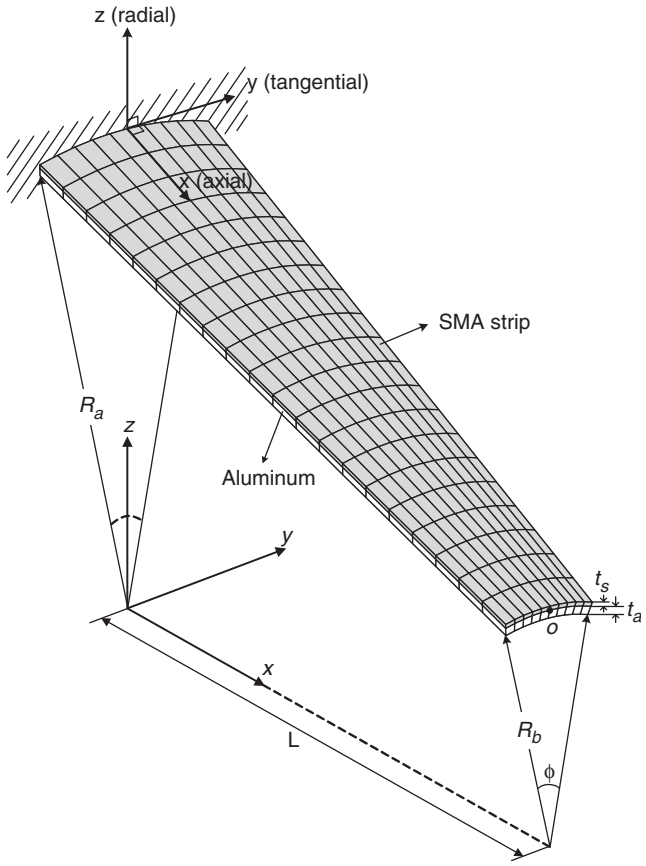

Figure 23. *FEM model of the conical shell structure with a SMA strip.*

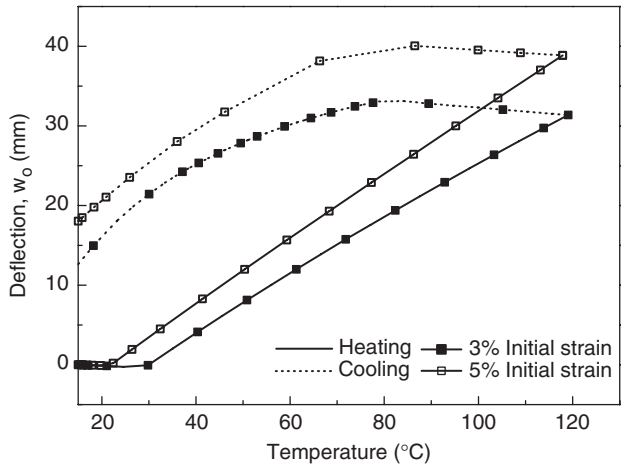

Figure 24. *Tip deflection vs temperature cycle on a SMA strip.*

combining strip SMA actuators are investigated. The numerical algorithm of the 3-D SMA thermomechanical constitutive equations based on Lagoudas model is developed to analyze the unique characteristics of SMA strip such as the pseudoelastic behavior and shape memory effect. The incremental SMA constitutive equations are implemented in the UMAT written by FORTRAN with ABAQUS finite element program. The shape change of structure is caused by the initially

Downloaded from jim.sagepub.com at KAIST GRADUATE SCHOOL OF MGMT on April 19, 2011

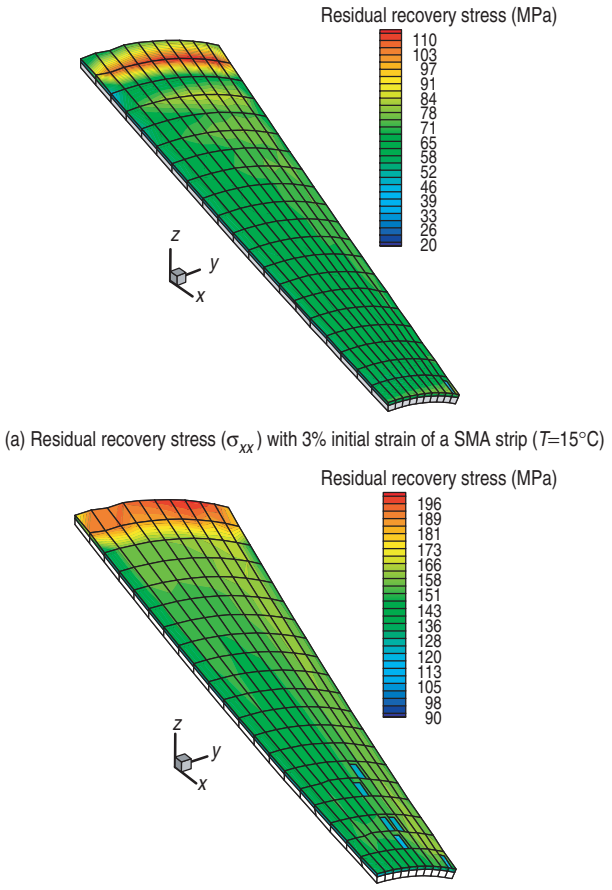

Figure 25. *Distribution of residual recovery stress (σ_{xx}) at the end of temperature cycle on SMA strip.*

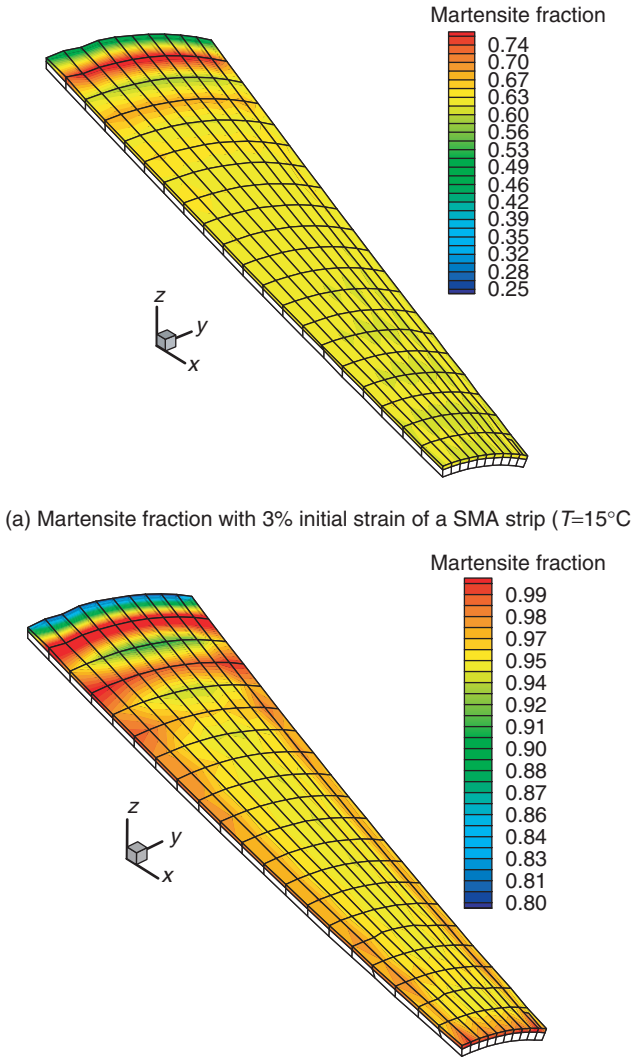

Figure 26. *Distribution of martensite fraction at the end of temperature cycle on SMA strip.*

strained SMA strip bonded on the surface of host structure when thermally activated. The SMA strip starts transformation from the martensitic into the austenitic state upon actuation through heating, simultaneously recovering the initial strain, thus making host structure to change the shape. Numerical results show that the SMA strip actuator can generate enough recovery force to deform the host structure and sustain the deformed shape subjected to large external load, simultaneously. In this study, the shape memory effect is restricted to one-way applications, unless the SMA is coupled to an elastic structure which compels the SMA to recover the initial condition. But the SMA strip might generate the residual recovery stress and does not fully recover its martensite fraction after the first loading cycle, even if the SMA is coupled to an elastic structure. Therefore, the deformed structure cannot fully recover its original shape due to residual recovery stress of SMA. Also, depending on the initial value of martensite fraction, SMA cannot be used as a reversible actuator because, martensite fraction cannot be recovered to its initial value. So, it is difficult to make a reversible shape adaptive structure using one-way SMAs and necessary to investigate the interactions between host structure and the SMA actuator. The two-way shape memory effect could be a solution to make the actuation reversible. However, if high precision is needed in terms of activation magnitude versus the number of cycles, the issues of thermal fatigue and drift in the response are still not completely solved. Therefore, the accurate prediction of the thermomechanical behavior of the SMA should be further studied to design the actuator and shape adaptive structure, taking into account the nonlinear and hysteretic behavior of the SMAs.

ACKNOWLEDGMENTS

This research was performed for the Smart UAV Development program, one of the 21st Century Frontier

Downloaded from jim.sagepub.com at KAIST GRADUATE SCHOOL OF MGMT on April 19, 2011

R&D programs funded by the Ministry of Science and Technology of Korea. The authors also acknowledge the support from the National Research Laboratory (NRL) program.

REFERENCES

Bathe, K.J., Ramm, E. and Wilson, E.L. 1975. "Finite Element Formulations for Large Deformation Dynamic Analysis," *International Journal for Numerical Methods in Engineering*, 9(2):353–386.

Boyd, J.G. and Lagoudas, D.C. 1996. "A Thermodynamical Constitutive Model for Shape Memory Materials. Part I. The Monolithic Shape Memory Alloys," *International Journal of Plasticity*, 21(6):805–842.

Brinson, L.C. 1993. "One-dimensional Constitutive Behavior of Shape Memory Alloys: Thermomechanical Derivation with Non-constant Material Functions and Redefined Martensite Internal Variable," *Journal of Intelligent Material Systems and Structures*, 4(2):229–242.

Hibbitt, H.D., Marcal, P.V. and Rice, J.R. 1970. "Finite Element Formulation for Problems of Large Strain and Large Displacement," *International Journal of Solids and Structures*, 6(8):1069–1086.

Kudva, J.N. 2004. "Overview of the DARPA Smart Wing Project," *Journal of Intelligent Material Systems and Structures*, 15(4):261–267.

Lee, I., Roh, J.H. and Oh, I.K. 2003. "Aerothermoelastic Phenomena of Aerospace and Composite Structures," *Journal of Thermal Stress*, 26(6):525–546.

Liang, C. and Rogers, C.A. 1990. "One-dimensional Thermomechanical Constitutive Relations for Shape Memory Materials," *Journal of Intelligent Material Systems and Structures*, 1(2):207–234.

Marfia, S., Sacco, E. and Reddy, J.N. 2003. "Superelastic and Shape Memory Effect in Laminated Shape-memory-alloy Beams," *AIAA Journal*, 41(1):100–109.

Ortiz, M. and Simo, J.C. 1986. "An Analysis of a New Class of Integration Algorithms for Elastoplastic Constitutive Relations," *International Journal of Numerical Methods in Engineering*, 23(3):353–366.

Qidwai, M.A. and Lagoudas, D.C. 2000. "Numerical Implementation of a Shape Memory Alloy Thermomechanical Constitutive Model using Return Mapping Algorithms," *International Journal for Numerical Methods in Engineering*, 47(6):1123–1168.

Roh, J.H. and Kim, J.H. 2003. "Adaptability of Hybrid Smart Composite Plate under Low Velocity Impact," *Composite Part B: Engineering*, 34(2):117–125.

Singh, K., Sirohi, J. and Chopra, I. 2003. "An Improved Shape Memory Alloy Actuator for Rotor Blade Tracking," *Journal of Intelligent Material Systems and Structures*, 14(12):767–786.

Sun, Q.P. and Hwang, K.C. 1993a. "Micromechanics Modeling for the Constitutive Behavior of Polycrystalline Shape Memory Alloys – I. Derivation of General Relations," *Journal of the Mechanics and Physics of Solids*, 41(1):1–17.

Sun, Q.P. and Hwang, K.C. 1993b. "Micromechanics Modeling for the Constitutive Behavior of Polycrystalline Shape Memory Alloys – II. Study of the Individual Phenomena," *Journal of the Mechanics and Physics of Solids*, 41(1):19–33.

Downloaded from jim.sagepub.com at KAIST GRADUATE SCHOOL OF MGMT on April 19, 2011